Latin American Journal of Solids and Structures
www.lajss.org

A Numerical and experimental study on the crash behavior of the extruded aluminum crash box with elastic support

Abstract
Thin-walled structures like crash boxes may be used as energy absorption members in automotive chassis. There have been many studies addressing the behaviors of energy absorption members on frontal crash. These researches have attempted to predict the energy absorption and maximum impact load in shell structures. The energy absorption and maximum impact load depend on many parameters including boundary condition, history of plastic deformation during metalworking, geometry; and material and impact energy (i.e. mass and velocity of the striker). This study examined the crash behavior of square tube made of the extruded aluminum alloy 6063T4 using an elastic boundary condition - instead of rigid boundary condition- on the bottom of a crash box, In addition, the effect of elastic boundary condition on energy absorption of square tubes under the impact load was investigated both numerically and experimentally. Results showed that using elastic boundary could change the deformation mode and decrease the maximum impact load. Further, a high correlation between the numerical and experimental results validated the findings of the study.

Keywords
Thin wall structure, Elastic support, Square tube, Peak load, Energy absorption

J. Marzbanrad*[a]
A. Keshavarzi[b]

School of Automotive Engineering,
Iran University of Science and Technology,
Tehran, Iran,
*[a] Corresponding author: marzban@iust.ac.ir
[b]ahmadkeshavarzi@iust.ac.ir

1 INTRODUCTION

Thin-walled beams are widely used as crash absorbers in automotive chassis. Such kinds of structures are frequently used in the front parts of the car. These members play an important role in energy absorption of the frontal crash. Thin-walled tubes absorb the kinetic energy of the crash by plastic deformation to protect the auto occupants. These elements are specifically designed to absorb high amounts of energy during a crash to ensure passenger cabin integrity and consequently, passenger safety. Therefore, the structure must be deformed by collapse and sequential folding process during plastic deformation. While collapsing the structure, the process of plastic deformation must be controlled to absorb as much energy as possible. As a result, a car with good crash absorber design and weight reduction could be desirable for the vehicle performance and competition in the market. So far, many scholars have conducted studies on modeling the behaviors of the thin-walled structures and promoting energy absorption under frontal crash.
The increasing demand for the lighter and more efficient energy absorbing structural components in transportation systems has made designers in automotive companies develop various methods. The

use of lightweight structures is one of the important methods for achieving the aforementioned goal. Nevertheless, it is required that the new lighter structures sustain or exhibit improved crash energy absorption. Multiple alternatives such as advanced high-strength steels, aluminum or magnesium alloys, and composite materials have been proposed for replacing mild steel in automotive structures, as stated by Luand Yu (2003).

Due to its low weight and corrosion resistor, Aluminum alloy is a good alternative that can be recycled with much less required energy than that needed to produce primary aluminum. The prospect shows that for example, in Europe, consumption of aluminum will increase to 30% until 2020as shown in Figure1. Accordingly, Galib (2006) analyzed the behaviors of aluminum alloy in crash using crash boxes with Aluminum alloy material.

The energy absorption and maximum impact load in aluminum crash box during a crash depend on many parameters such as geometry, strain-rate sensitivity, history of plastic deformation during metalworking, porosity of material, temperature during crash, boundary condition and impact energy (mass and velocity of striker).

Alexander (1960), Pugsley (1960), Karagiozova and Alves (2004), Karagiozova and Jones (2008), and Abramowicz, Jones (1986) studied aluminum section with various geometrical features such as circle; Abramowicz and Jones (1984), Najafi and Rais-Rohani (2011), Rossi and Behdinan (2005); Aktaya, Kröplin, Güden (2008), Güden and Kavi (2006) studied the rectangular sections. Bouchet, Jacquelin E, Hamelin (2002), El-Sobky, Singace (1999) investigated double chamber extrusions, while Zhang and Huh (2009), Salehghaffari et al. (2010) on grooved tubes. Marzbanrad et al. (2009), Adachi et al. (2008), JandaghiShahi and Marzbanrad (2012), Zhang and Suzuki (2007) presented their works on tubes stiffened by stringers or rings; similar structures with dents or bellows, curves and other types of aluminum alloy (e.g. 6063 T3/T4/T6/T7 and EN AW-7108 T6) are used as crash box and energy absorbers in front of the car.

Crash box structure has a history of plastic deformation during metalworking which also affects the response during a crash. After rolling, sheets pass several operations such as tension, bending and stretching with different loading paths which are carried out at different strain rates. Thus, the dynamic response of the crash box is affected by the history of pre-plastic deformation, an issue addressed by many scholars. In this study, 6063, whose history of pre-plastic deformation is unknown, was used and it was attempted to calculate this characteristic at different strain rates to increase the accuracy of numerical modeling.

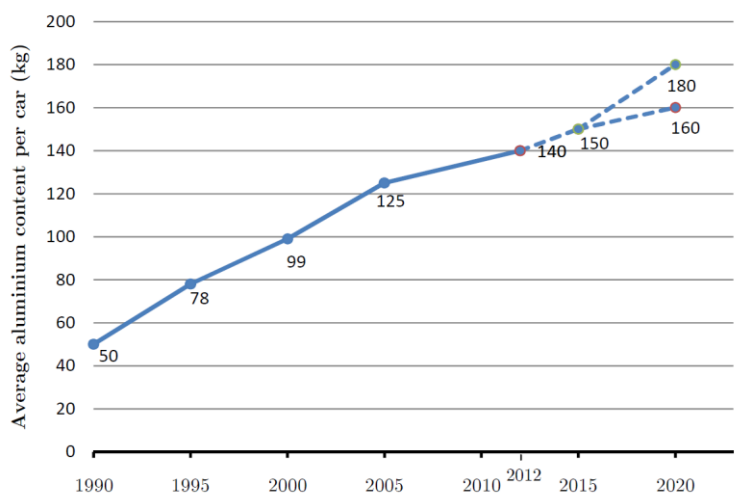

Figure 1: Evaluation of average aluminum content per car produced in Europe[1]

[1]Source: *European aluminum association*

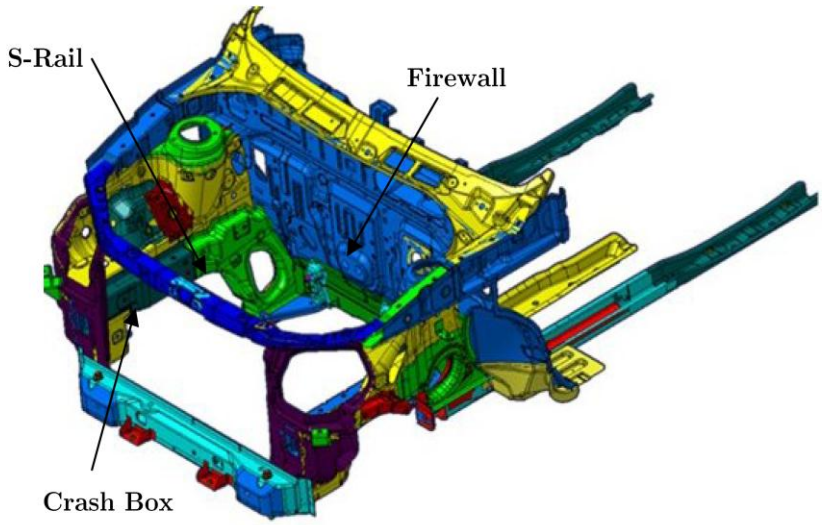

Figure 2: Front body panel assembly of Tiba (Saipa Group)

In most related studies, the crash box structure with one rigid support in one side is considered. However, this support is not rigid in real condition, because the attached structure of vehicle such as s-rail and firewall to this support are flexible (Figure 2). In aerospace industry, the crash with soft soil or water under distributed loading was introduced by Lankarani and Ramalingam (2002) and Nagnhipour et al. (2008). These scholars found that types of support have important impacts on the behavior of the structure at crash. By considering s-rail and firewall as soil or water, this structure in our study was assumed as an elastic support. Finally, numerical results can be precisely followed by the experimental outcomes.

The aim of this study was to give a set of experimental and numerical results of crash tests on aluminum square extruded. This series of tests served to (a) generate experimental data for the validation of numerical simulations; (b) study the effect of elastic support on the dynamic behavior of aluminum 6063T4,

The main objectives of this research were: (1) presenting a set of experimental results of crash test on aluminum square extruded and validating a numerical simulation for static and dynamic axial crushing of square aluminum extrusions in alloy 6063 temper T4; (2) studying the static and dynamic behavior of square thin-walled tubes subjected to axial loading with variable support stiffness and impact velocity values; (3) validating the numerical prediction of the crushing behavior using the experimental results obtained previously; and (4) gauging the effect of elastic support on the behavior and the deformed shape of these tubes.

2 EXPERIMENTAL SET-UP

The experimental tests were conducted on dynamic test rig arrangement, as can be observed in Figure3. They were designed, and installed in the laboratory of automotive structure in Iran University of Science and Technology. This test rig had a mass (140 to 500 kg) which could slide on 10m rail, resulting in a maximum impact speed of 13 m/s. The mass of striker in this research was 150kg.Toinvestigate the effect of velocity on the dynamic response of squared tube; three velocities for striker velocity were selected: 5, 5.5 and 7 m/s.

Figure 3: Crash box test rig

2.1 Data acquisition system

The load, acceleration and displacement data were recorded with a PC using the two portable data acquisition systems, Advantech USB4716 card and InnoBeamer-L2.The Advantech USB4716 card for collecting load and displacement data and theInnoBeamer-L2 for acceleration data. The load was measured using load sensor (CDIT-1) attached to anvil. The acceleration was measured using an accelerator sensor (VMI-102) attached to the striker, Also, laser displacement sensors provided the axial deformation distance of the tubes and the initial impact velocity. Crash test data was filtered to a Channel Frequency Class (CFC) of 180 Hz according to SAE J211, which is the standard practice for the analysis of crash test accelerometer data. Figure 4 displays the experimental set-up with all schematic arrangements.

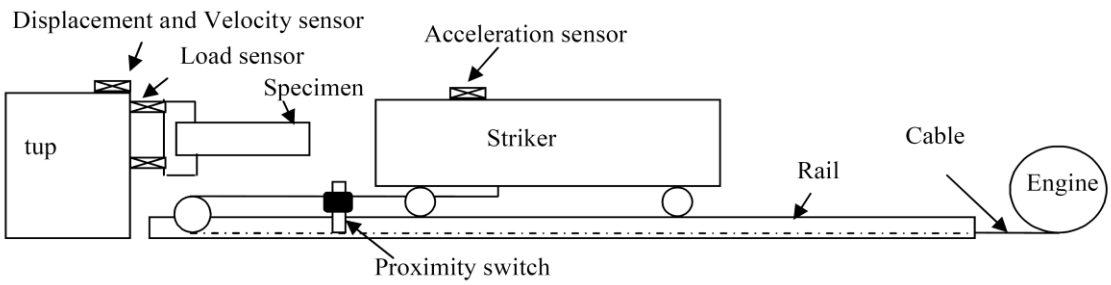

Figure 4: Schematic of crash box test rig

.

2.2 Measurement System architecture

The architecture of the proposed measurement system is shown in Figure 5 .The system is composed of five level structures:

- Graphic interface
- General boards
- Application board
- Engine control unit
- Power supply

There is at the top level of the system architecture a graphic interface (GI). The whole measurement system and engine control unit is controlled through the GI which can be customized according to the user's requests. The connection between general board and GI is implemented by the universal serial bus (USB) protocol. Visual c sharp is used to develop GI. The GI starts the engine, selects a gear (by control a pneumatic cylinder on the gearbox and on the clutch system), set a crash velocity (with throttle control by servo motor), stores and processes the measured data, calculate a crash important parameter (energy absorption) and show measurement data versus time.
A general boards which include the three boards; M302 VibroMetra card, Advantech USB4716 card and Haidenhain IK220 counter card. A Hall Effect switch on the trolley made active InnoBeamer-L2cardand the Advantech USB4716 when trolley is near the test specimen then InnoBeamer-L2cardsaves data that generated from acceleration sensor that located in trolley and The Advantech USB4716 save data from load cell and displacement sensor.
A servo motor on throttle valve controls the angular velocity of crank shaft. A Hall Effect sensor in the crank shaft reports the angular velocity to the Haidenhain IK220 counter card by the number of the pulses per sampling time. There are three relay on the engine control unit to active start, Solenoid 3/2 pneumatic valve on the gearbox to change gear and on the clutch for start a movement of trolley on the rail.

2.3 Software management

At the top level of the system architecture inFigure5 we have the system manager, the personal computer. The whole measurement system is controlled through a graphic interface, which can be customized according to the user's requests. The user can interact with a windows-like interface, by defining the desired measurement conditions. After each crash test, the data of load, acceleration, velocity and displacement were saved and transferred to software developed for this test. This software includes a Kalman filter to remove the quantization and process noises in the measurement.
This software could calculate parameters such as energy absorption of the tube, E_{ab}, the maximum crush load, P_{max}, the mean crush load, P_{mean} and the crush load efficiency (CFE). E_{ab} is defined as the external work of the tube, which can be calculated as follows:

$$E_{ab}=\int P(\delta)d\delta \tag{1}$$

The first peak is the peak crash load, P_{max}; and the area under the crash load–displacement curve is the absorbed energy. The mean crushing load was defined as the absorbed impact energy per unit axial deformation of a specimen and calculated for each part as following:

$$P_m=\frac{1}{\delta}\int_0^{\delta}P(\delta)d\delta \tag{2}$$

The integral in (2) refers to the area under load-displacement curve that is representative of the amount of absorbed energy; and $d\delta$ is the total displacement. In other words, P_m is the absorbed energy per unit length.
Crush load efficiency, CFE, which is an important criterion for comparing energy absorber capabilities, is defined by AlaviNia et al. (2012) as:

$$CFE=\frac{P_m}{P_{Max}}\times 100 \tag{3}$$

P_m and P_{max} are two main parameters for the description of absorbers' characteristics. The greater value of P_m corresponds to the larger value of the absorbed energy as a desired property. On the other hand, attempts have been made to decrease the value of the peak load, P_{max}. CFE is a very important parameter in the design of energy absorbers; accordingly, the higher values mean that the absorber has the good capability of energy absorption associated with low peak load; thus, it is the best criterion for comparison.

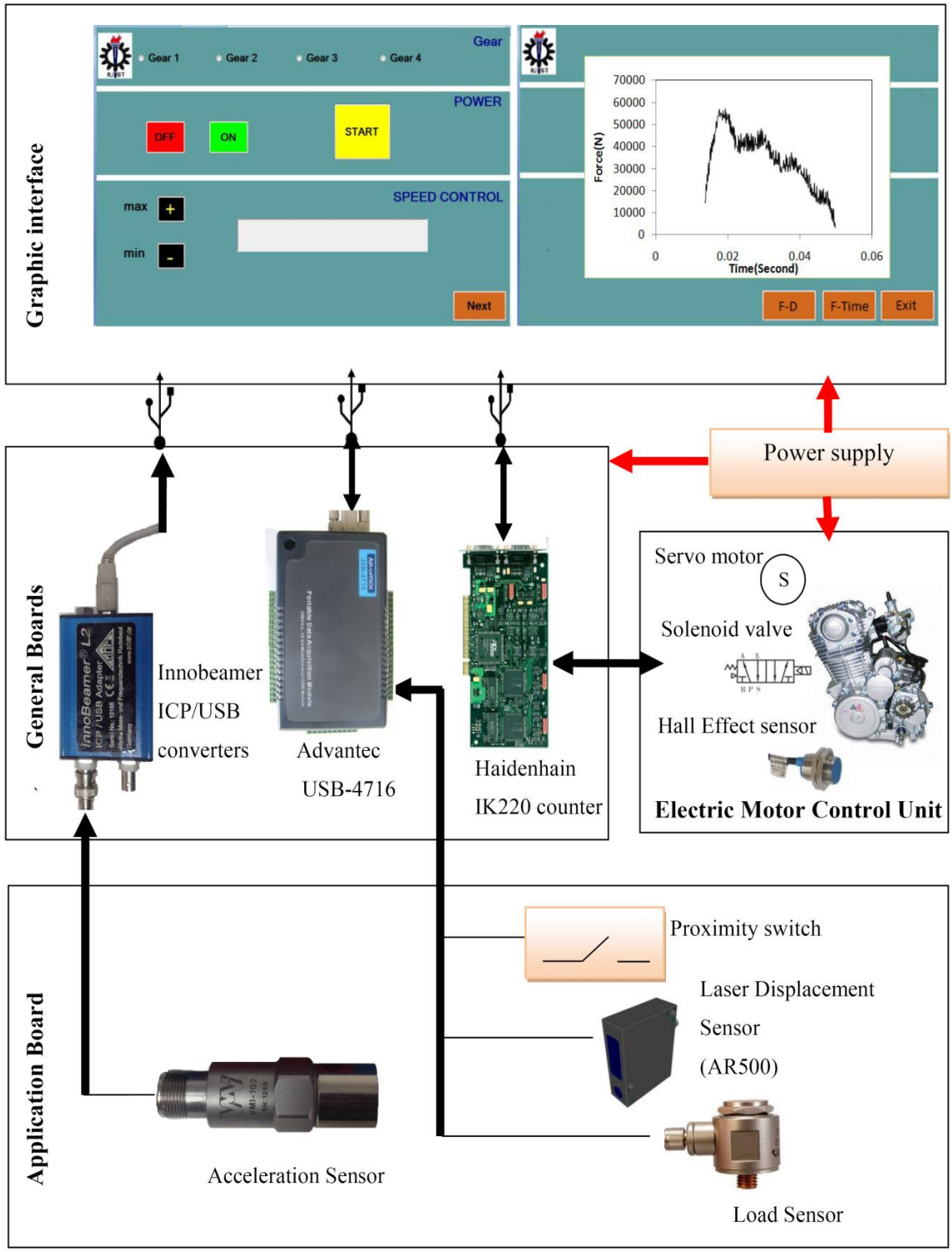

Figure 5: Architecture of Measurement and engine control system

3 NUMERICAL ANALYSIS

The finite element commercial software ABAQUS/Explicit has been used to study the numerical simulations. Four-node shell elements with reduced integration (ABAQUS S4R) were employed to model the square box tests with AA6063-T4. The effect of the element size on computational results and CPU time was checked; a 1.9mm×2mm element showed reasonable results.

The striker was regarded as a point mass attached to a rigid surface with 150 kg weight and the initial velocity (V_0) in x direction. The bottom of tube was clamped in a rigid plane resembling the rigid support in this modeling. The contact between the tube and the striker was defined as the surface to surface interaction with a friction coefficient of 0.2. Besides, self-contact was defined as the whole tube surface.

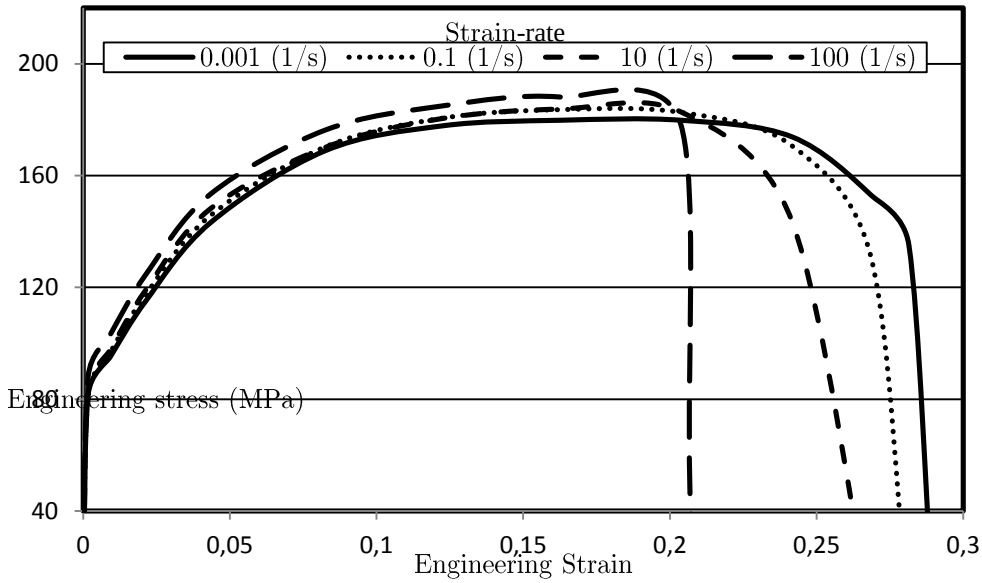

Figure 6: Engineering stress-strain curve at four different strain rates

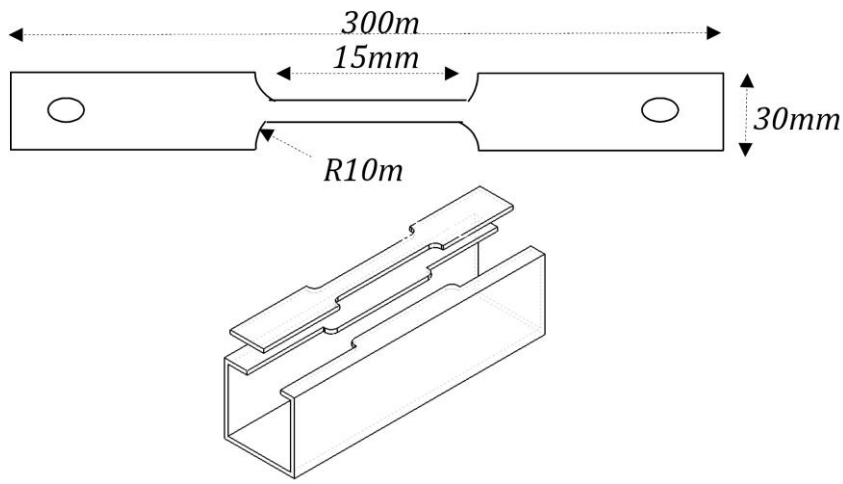

Figure 7: Specimen geometry

The material was stain-rate sensitive aluminum alloy (6063-T4) with young's modulus and density of E=68.9 GPa and ρ=2700kg/m3, respectively. The Cowper-Symonds overstress power law equation was used to determine the material's constitutive equation that contained specific material constants and parameters obtained experimentally. Equation (4) describes the Cowper-Symonds power low equation as stated by Jones (1997) as:

$$\frac{\sigma_d}{\sigma_0}=1+\left(\frac{\varepsilon_r}{D}\right)^{1/q} \tag{4}$$

where σ_d is the dynamic yield stress,σ_0 is the static yield stress that is 89.6 MPa for aluminum alloy 6063T4,ε_r is the strain rate, D and q are material parameters. To determine parameters in Cowper-Symonds equation, a series of tensile tests at different strain rate had to be conducted. Stress-strain curve was gained using STM-150 Cap.150 KN for four different stress-strain velocities. To simulate strain stress sensitivity, aluminum 6063T4 box was used in the dynamic test. The investigation was done with AST-150 to extract the data. Figure 6 shows engineering strain versus strain at strain rates of 10, 50, 100 and 200s^{-1}. The tests conducted at 23 ^{o}C for all four strain rates, and three specimens were run at each set of conditions. The specimen geometry used in all experiments is shown in Figure 7.Specimenswere cut along the longitudinal direction of the tubing as 30 mm wide strips by 300 mm long.

The determined values of two specific material parameters for Aluminum 6063T4 were D=6952.399and q =16828. By putting the two material parameters into the Equation (4), the Equation (5) was obtained. Figure 8 shows the comparison of the measured curve tested:

$$\frac{\sigma_d}{\sigma_0}=1+\left(\frac{\varepsilon_r}{6952.399}\right)^{1/1.6828} \tag{5}$$

The dimensions of the tubes were: L=300mm, b=54mm and the wall-thickness, t=2 mm. In this study, two models have been applied for the analysis of numerical results; a) a tube with rigid support and b) a tube with elastic support that seemed to be closer to the reality. The rigid and elastic supports are shown in Figure 9. A spring element was used at the back of the bottom plane for modeling elastic support in this case. A diaphragm spring was used in the experimental analysis, and it was welded to anvil Figure 10 shows a sample with elastic support in this apparatus crash test. Dimension of this spring is shown in Figure 11. The spring characteristic was varied within wide limits by altering the ratio of free cone height h_0 to thickness t (Almen and Laszlo).The load-deflection characteristics of diaphragm spring are showed in the Figure 12. Three diaphragm springs were used in this test by series stacking. The Experimental results showed that the Maximum spring deflection at impact with velocity7.5 m/s was 3.92 mm. According to the obtained data, the nonlinear equation between spring deflection and load was linearized between 0 to 4mm.The stiffness of spring was considered34194kN/min the numerical study for triple spring.

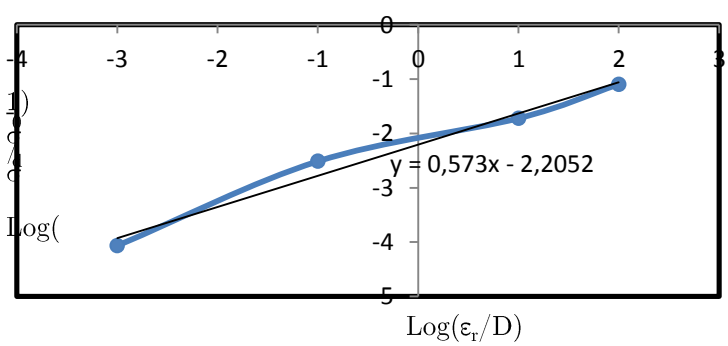

Figure 8: Comparison of the simulated curve with the measured curve at 23 ^{o}C

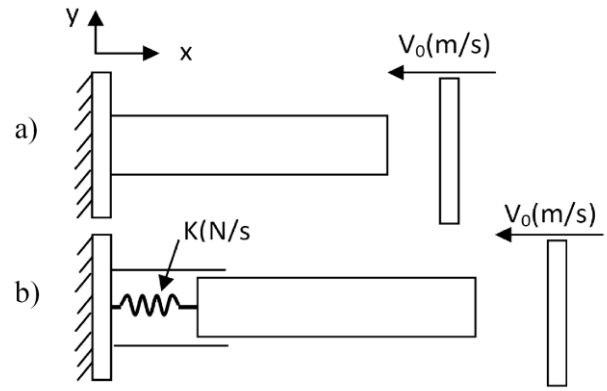

Figure 9: Two types of boundary conditions a) the solid support, b) the elastic support

Figure 10: An elastic support in the manufactured apparatus

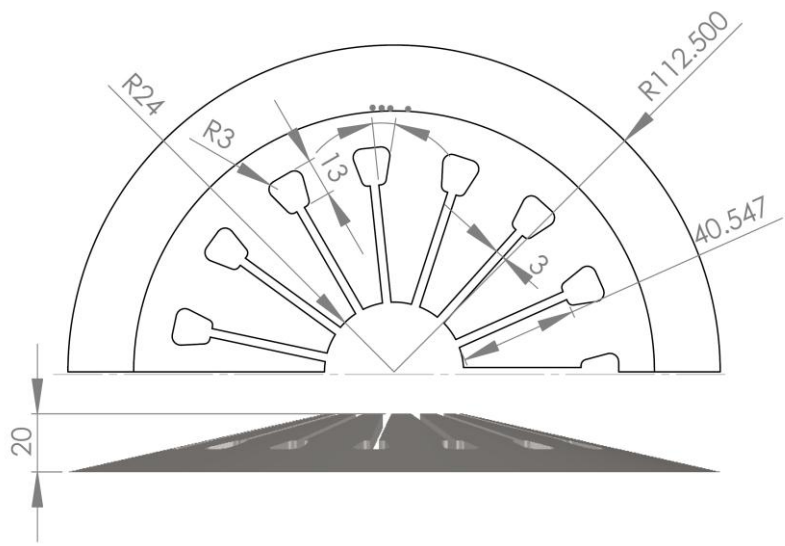

Figure 11: A section of diaphragm spring used in the experimental analysis

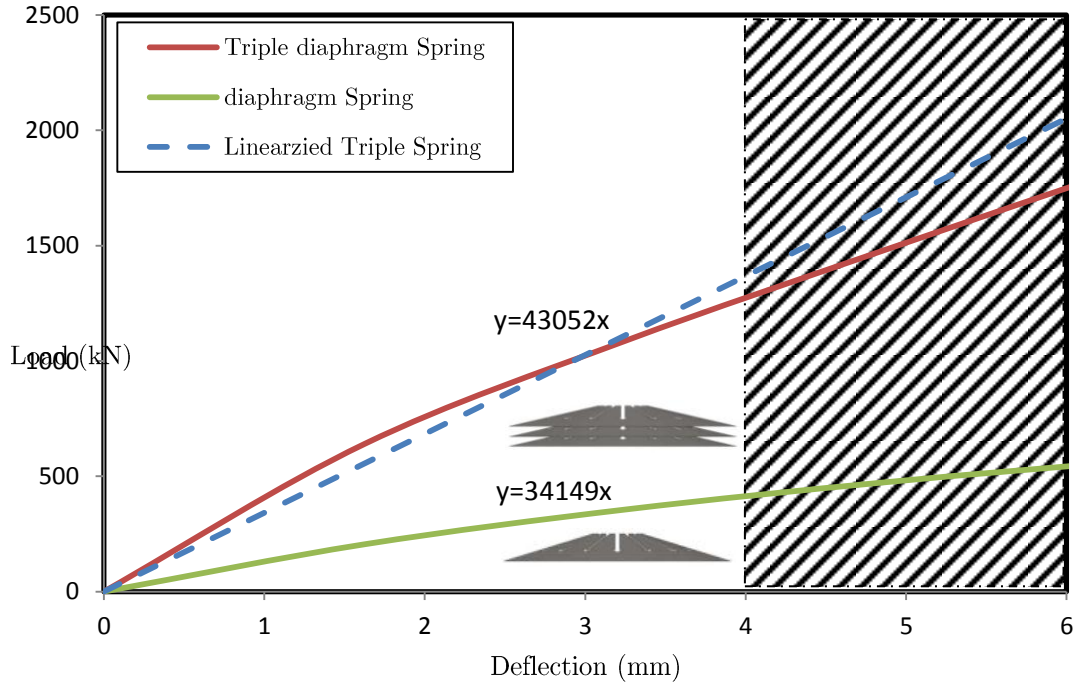

Figure 12: A section of diaphragm spring used in the experimental analysis

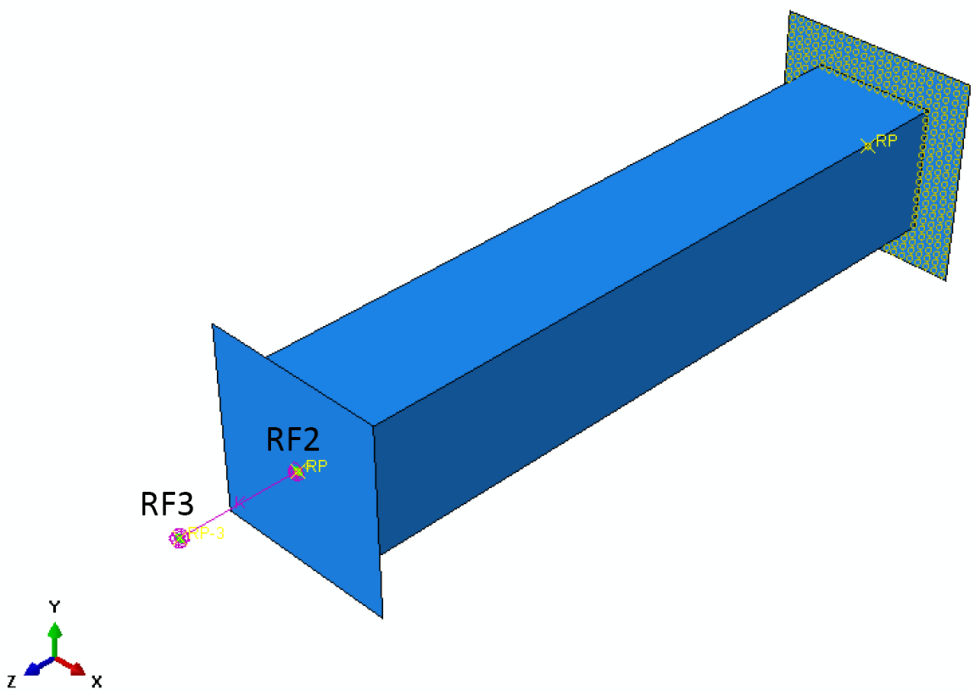

Figure 13: Numerical model used in Abaqus software

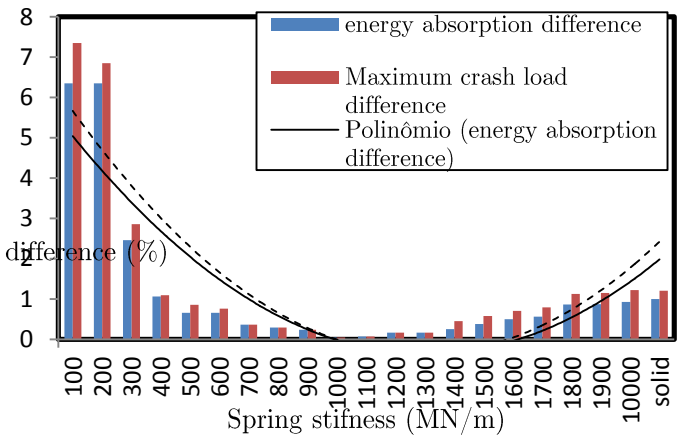

Figure 14: Difference between energy absorption and crash load of experimental rigid wall support and a series of elastic support in numerical simulation

To find stiffness near to experimental stiffness for rigid wall, first all of freedom degree of support reference point (RF2) is fixated as illustrated in Figure13;then the difference between energy absorption (de) and maximum crash load (dl) is calculated as Equations (6) and (7).

$$\text{de}=\left|100 * (E^{N}_{k=\infty} - E^{E}_{k=real})/E^{N}_{k=\infty}\right| \tag{6}$$

$$\text{dl} = \left|100 * (ML^{N}_{k=\infty} - ML^{E}_{k=real})/M^{N}_{k=\infty}\right| \tag{7}$$

Where the parameters are:

$E^{N}_{k=\infty}$	Energy absorption with fixed RF2	$\text{ML}^{\text{N}}_{\text{k=}\infty}$	Maximum crash load with fixed RF2
$E^{E}_{k=real}$	Real Energy absorption a crash box with rigid wall	$\text{ML}^{\text{E}}_{\text{k=real}}$	Real maximum a crash box with rigid wall

The result of experiment and numerical simulation is illustrated the absolute difference within 1.2% for energy absorption and within 1.5% for maximum crash force. For calculation the real and acceptable stiffness value for the rigid support in the experimental, z direction is applied free for RF2 (in software), then the spring element is used between RF2 and RF3, and incrementally the stiffness of this element spring change until approaches to the experimental value of rigid wall. Difference between energy absorption and crash load of experimental rigid wall support and a series of elastic support in numerical simulation has been shown in Figure 14, which presents the best selected value is 1000MN/m.

4 RESULTS

4.1 Experimental and numerical results

Aluminum square tubes with length, edge and thickness of 300 mm, 45 mm and 2 mm respectively were used in this study. Six types of these specimens were prepared for testing: three tests with the rigid wall support (A series) and three tests for the elastic support (B series).Figure 15 shows the specimens after crash test.

Figures 16, 17 and 18 show the typical numerical and experimental results. The upper graphs show the crush load history, the middle graphs show the crash load-displacement, and the lower graphs represent the history of energy absorption during the crash. It can be deduced from Figure 14 (a) that at t = 0.02 s, the striker impacts the top edge of the tube, and at t = 0.02018 s, the stress wave reaches the bottom of the tube in series A and then, it is almost doubled (for this material,

elastic wave speed$C_0 = \sqrt{E/\rho} \approx 1597 m/s$). In series B, with the elastic support at t=0.02018 s, the stress wave reaches the bottom of the tube.

Between t = 0.2018 ms and t = 0.0375 s, the tube is compressed axially and the impact force has a plateau in which the entire square tube is deformed plastically. After t= 0.0375 s, the plastic region will be localized in the regions close to the folds. The impact velocity between A3 and B3 (Figure 16) and A2 and B2 (Figure 15) is only 0.5 m/s and the time data sequel in Figures 16 and 17 are the same.

Figure 18 (a) shows that the striker impinges the top edge of the tube at t = 0.0125 s and at t=0.0126 s, the stress wave reaches the bottom of the tube in A-series and then it is almost doubled. In B-series with elastic support at t=0.0126 s, the stress wave reaches the bottom of the tube. Between t = 0.0126 s and t = 0.0225 s, the tube is compressed axially and the impact force possesses a flat surface in which the entire square tube is deformed plastically. After t=0.0225 s, the plastic region will be localized in regions close to the folds.

The numerical simulation can truly predict the deformation mode, the maximum axial deformation (ultimate displacement), maximum crash load and the mean crash load. However, the numerical crash load is somehow different from the experimental result. Overall, it can be seen that there is the maximum difference at the highest degree of variance between the maximum crash load in numerical and experimental data. This difference could be either due to the friction effect of the sled on the rail, which possibly leads to energy absorption, or other errors concerning measurement-instruments.

The data of peak crash load (P_{max}), mean crash load (P_m), energy absorption (E_{ab}), maximum axial deformation (Δ) and crash force efficiency (CFE) are listed in Table 1. This table shows that there are no significant differences between experimental and numerical results. The peak crash load of specimens with elastic support (e.g. specimens A) is higher than those of rigid walls (e.g. specimens B), while mean crash load is being reversed. The maximum axial deformation (Δ) of sample A is higher than the one for sample B. The energy absorption of specimen with the rigid wall support is higher than specimen with elastic support; this is because compared to specimens with rigid support, specimens with the elastic support have a lower deformation. The CFE of specimens with the elastic support is lower than that of rigid support. It can be concluded that these specimens with elastic support have a small capability of energy absorption associated with the low peak load.

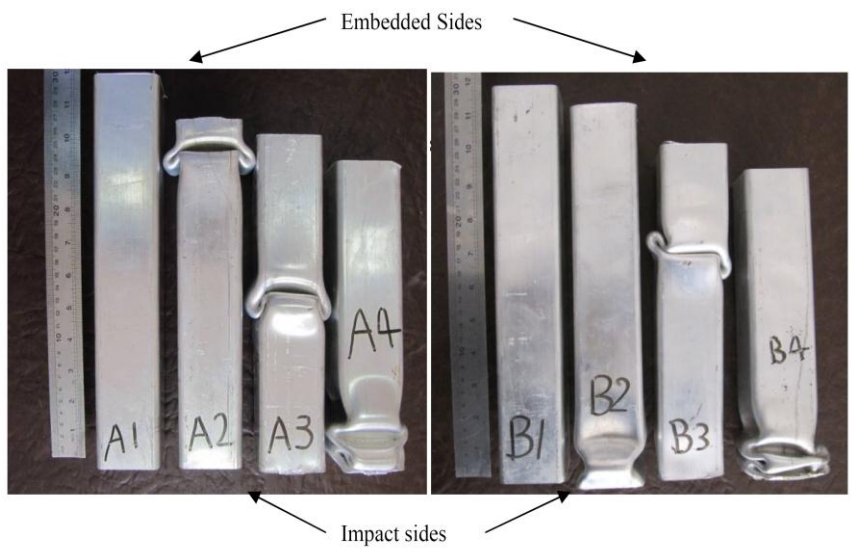

Figure 15: Tubes after tests

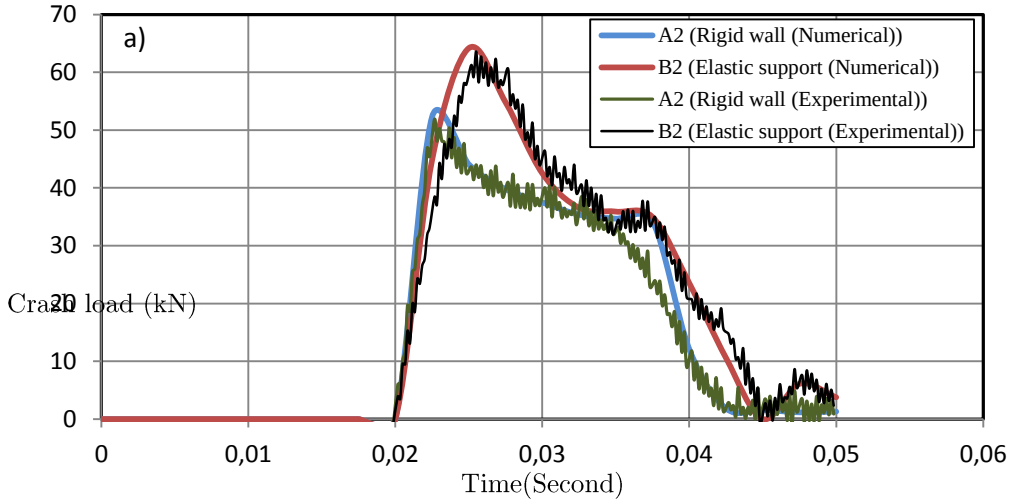

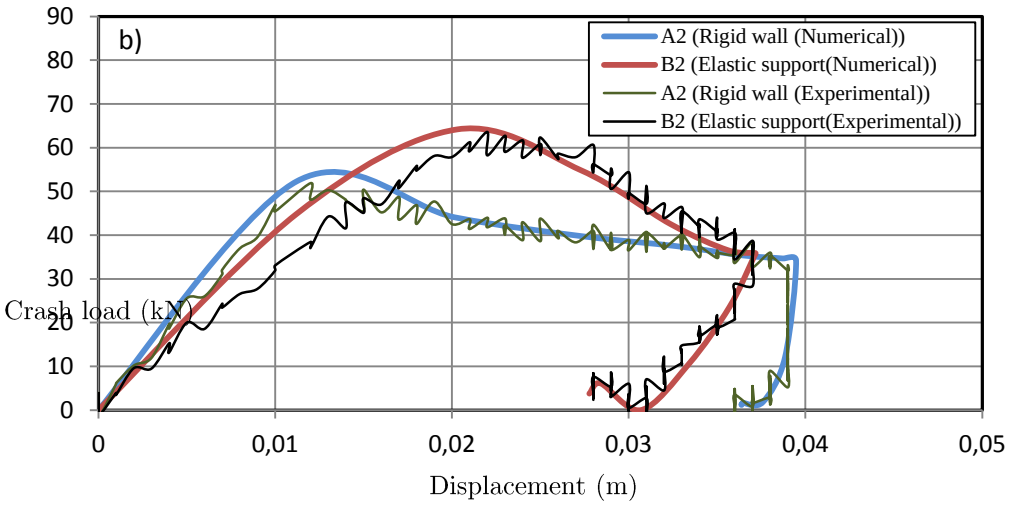

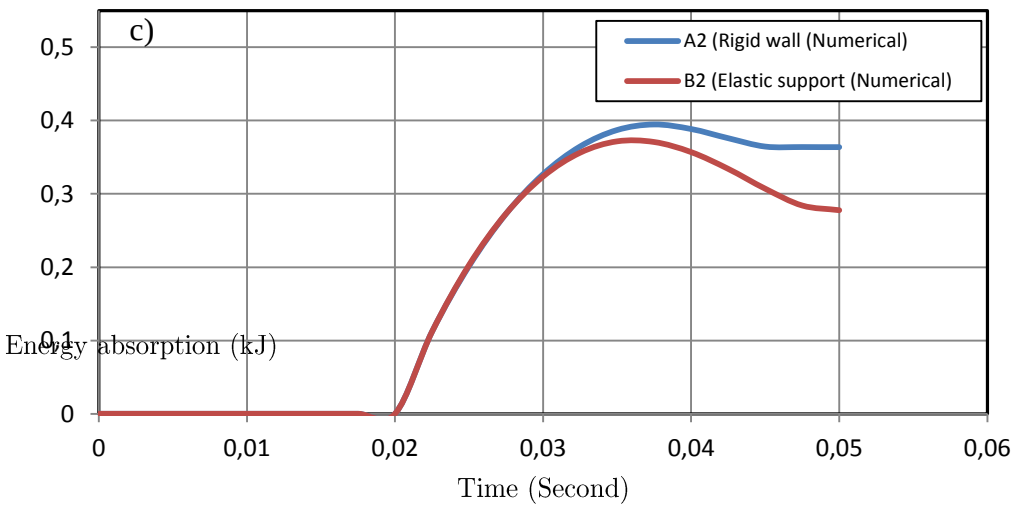

Figure 16: Experimental and numerical results of specimens A2 and B2. a) Crash load–crash time curve b) crash load–displacement curve c) Energy absorption

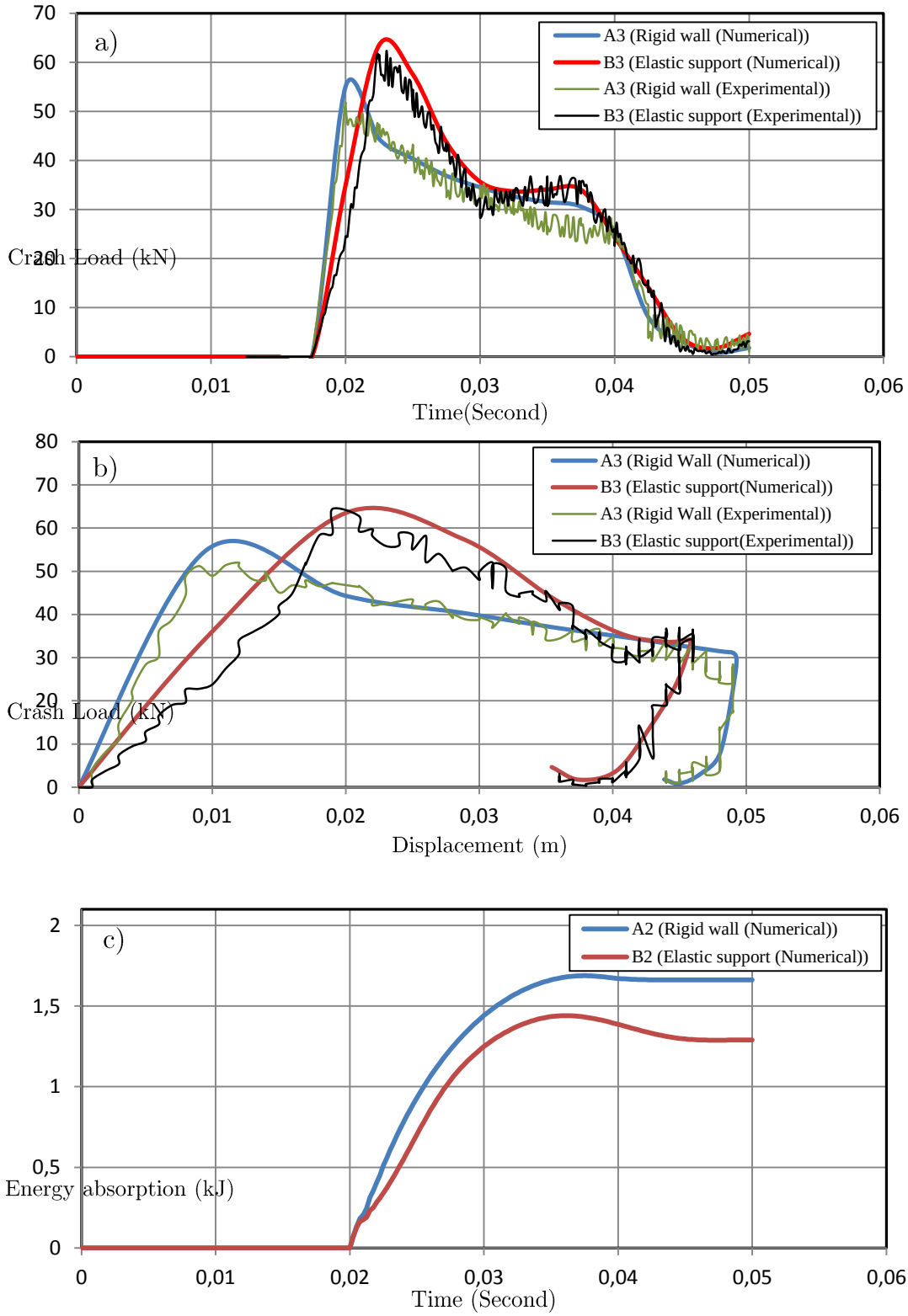

Figure 17: Experimental and numerical results of specimens A3 and B3. a) Crash load–crash time curve b) Crash load–displacement curve c) Energy absorption

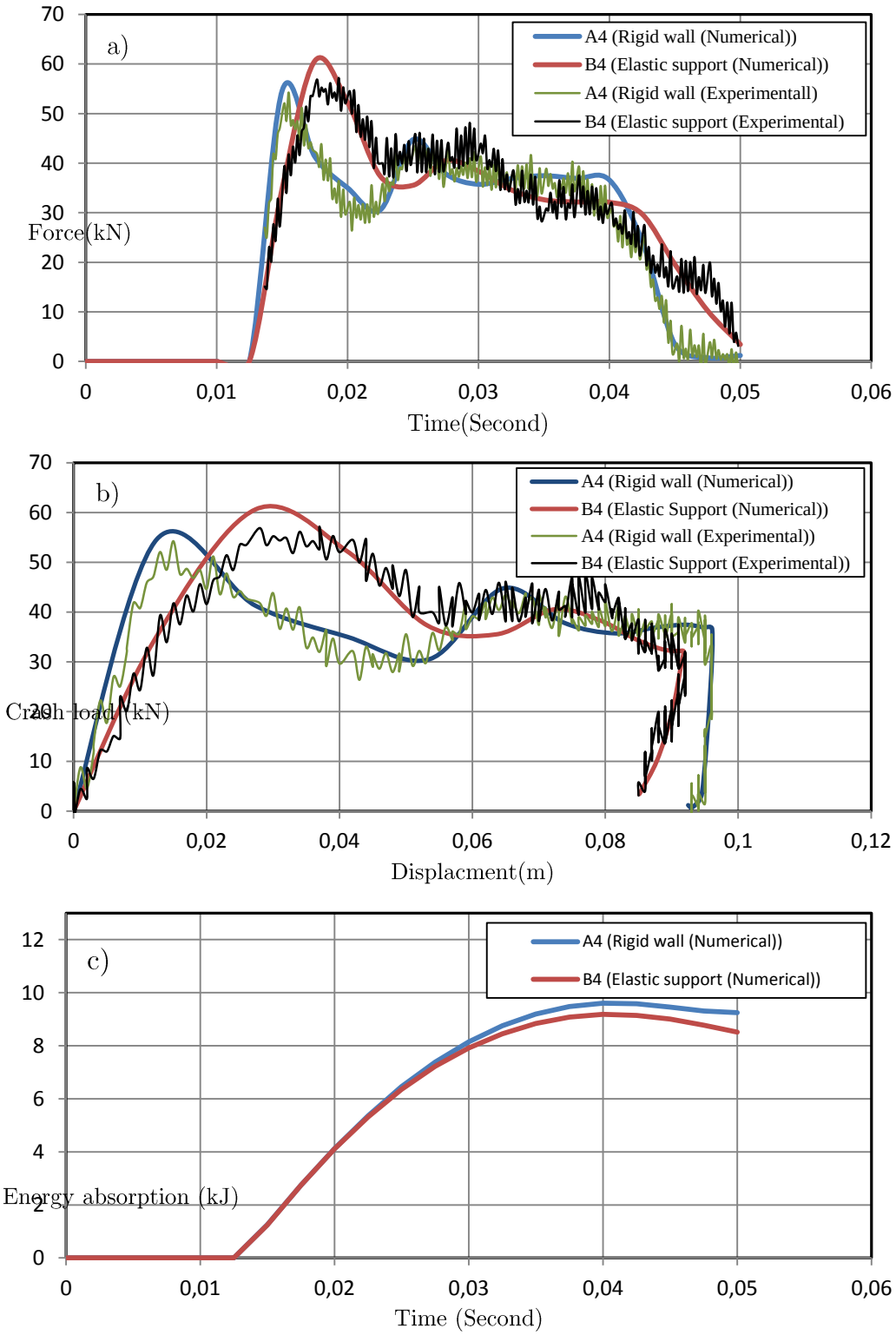

Figure 18: Experimental and numerical results of specimens A4 and B4. a) Crash load–crash time curve b) Crash load–displacement curve c) Energy absorption

Table 1: Comparison between experimental and numerical dynamic crash results

Test no.	V (m/s)	Impact mass (kg)	P^{E}_{mean} (N)	P^{N}_{mean} (N)	P^{E}_{max} (N)	E^{E}_{in} (J)	E^{N}_{in} (J)	Δ^{E} (mm)	Δ^{N} (mm)	CFE^{E} (%)	CFE^{N} (%)
A2	5	150	14160	14760	54029	353	363.76	24.05	24.65	32.8	31.28
A3	5.5	150	16880	17220	57457	425.2	438.55	25.1	25.46	29.9	28.23
A4	7.5	150	20792	22820	53898	912.2	924.68	43.8	40.52	38.5	41.78
B2	5	150	16100	17790	65835	268.3	277.73	16.6	15.61	30	30.19
B3	5.5	150	19127	19180	65740	344.3	354.26	18.0	18.47	27.5	27.72
B4	7.5	150	21694	24614	65740	837.3	851.21	38.59	34.58	37.6	40.6

4.2 Stiffness effect

The elastic support was modeled by springs with stiffness coefficient of K. Models of elastic support as well as the importance of support type will be presented in the obtained results. Thus, by applying changes in the spring stiffness coefficient, the elastic supports were compared in different situations. It is obvious that by increasing the stiffness to the infinity, it would be possible to achieve a state close to the rigid support.

In other to investigate the influence of crash box stiffness and elastic support stiffness on the energy absorption, a dimensionless numbers defined as stiffness ratio. Stiffness ratio is stiffness of crash box on the stiffness of elastic support. Stiffness of crash box is nonlinear and it depended on the velocity of crash. A mean stiffness is used in the stiffness ratio; this number is obtained by the flowing equation:

$$\bar{k} = 2E_{\text{energy absorption}}/D_{max} \tag{8}$$

D_{max}: Maximum crash box deformation

The Stiffness ratio in 5 and 10 m/s crash velocity is calculated in table2.

The various modes of the stiffness ratio are shown in Figure 19. As can be seen, the change in stiffness ratio coefficient causes the different energy absorption. Generally, if the stiffness ratio in the elastic support is decreased, energy absorption of the tube is increased, and the stiffness ratio≅0 (rigid support) has the maximum energy absorption.

The maximum deformation has also been plotted in Figure 20. These figures show that the deformation status can be completely different for each stiffness ratio coefficient; therefore, it is concluded that it may be possible to optimize the stiffness ratio in order to obtain the maximum axial deformation. It can be concluded in the 5m/s crash velocity (figure 20a),the range of 0.0329-0.0652 is better to consider for the stiffness ratio, also in the 10m/s crash velocity(figure 20b), the stiffness ratio is better to select small than 0.0007.

Table 2: table of data

	Crash Velocity =5m/s				Crash Velocity =10m/s			
Elastic Support Stiffness (MN/m)	Energy Absorption (J)	Maximum Deformation (mm)	Crash Box Stiffness (MN/m)	Stiffness Ratio	Energy Absorption (J)	Maximum Deformation (mm)	Crash Box Stiffness (MN/m)	Stiffness Ratio
5	6570	53.4	4.608004	0.9216	11826	179.5	0.734073	0.1468
6.25	6592	53.15	4.667031	0.7467	11865.6	180.15	0.731225	0.1170
7.5	6614	52.9	4.72697	0.6303	11905.2	180.8	0.7284	0.0971
8.75	6638.5	51	5.104575	0.5834	11949.3	179.75	0.739664	0.0845
10	6663	49.1	5.527603	0.5528	11993.4	178.7	0.751144	0.0751
17.5	6683	52.35	4.877172	0.2787	12029.4	179.45	0.747114	0.0427
25	6703	55.6	4.336603	0.1735	12065.4	180.2	0.743125	0.0297
37.5	6711	59.9	3.740792	0.0998	12079.8	181.25	0.735417	0.0196
50	6719	64.2	3.260353	0.0652	12094.2	182.3	0.727836	0.0146
62.5	6734.5	64.65	3.22254	0.0516	12122.1	180.35	0.745376	0.0119
75	6750	65.1	3.185457	0.0425	12150	178.4	0.763513	0.0102
87.5	6752	64.6	3.235917	0.0370	12153.6	174.9	0.794612	0.0091
100	6754	64.1	3.28757	0.0329	12157.2	171.4	0.827641	0.0083
300	6754.5	57.95	4.022688	0.0134	12158.1	176	0.785001	0.0026
500	6755	51.8	5.034958	0.0101	12159	180.6	0.745577	0.0015
750	6756	48.7	5.697203	0.0076	12160.8	182.15	0.73305	0.0010
1000	6757	45.6	6.499115	0.0065	12162.6	183.7	0.720839	0.0007
5500	6757.5	46.45	6.263897	0.0011	12163.5	182.6	0.729604	0.0001
10000	6758	47.3	6.041237	0.0006	12164.4	181.5	0.738529	0.0001

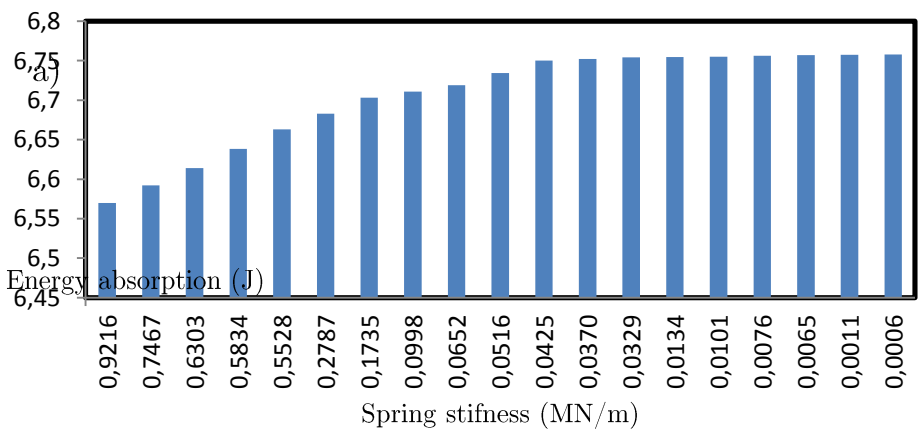

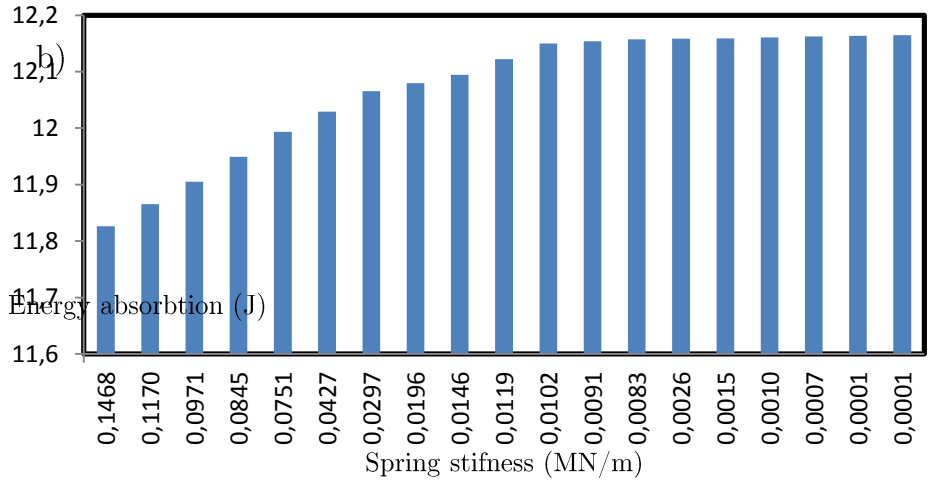

Figure 19: Energy absorption vs. different stiffness ratio, a) Impact velocity= 5 m/s b) Impact velocity=10 m/s

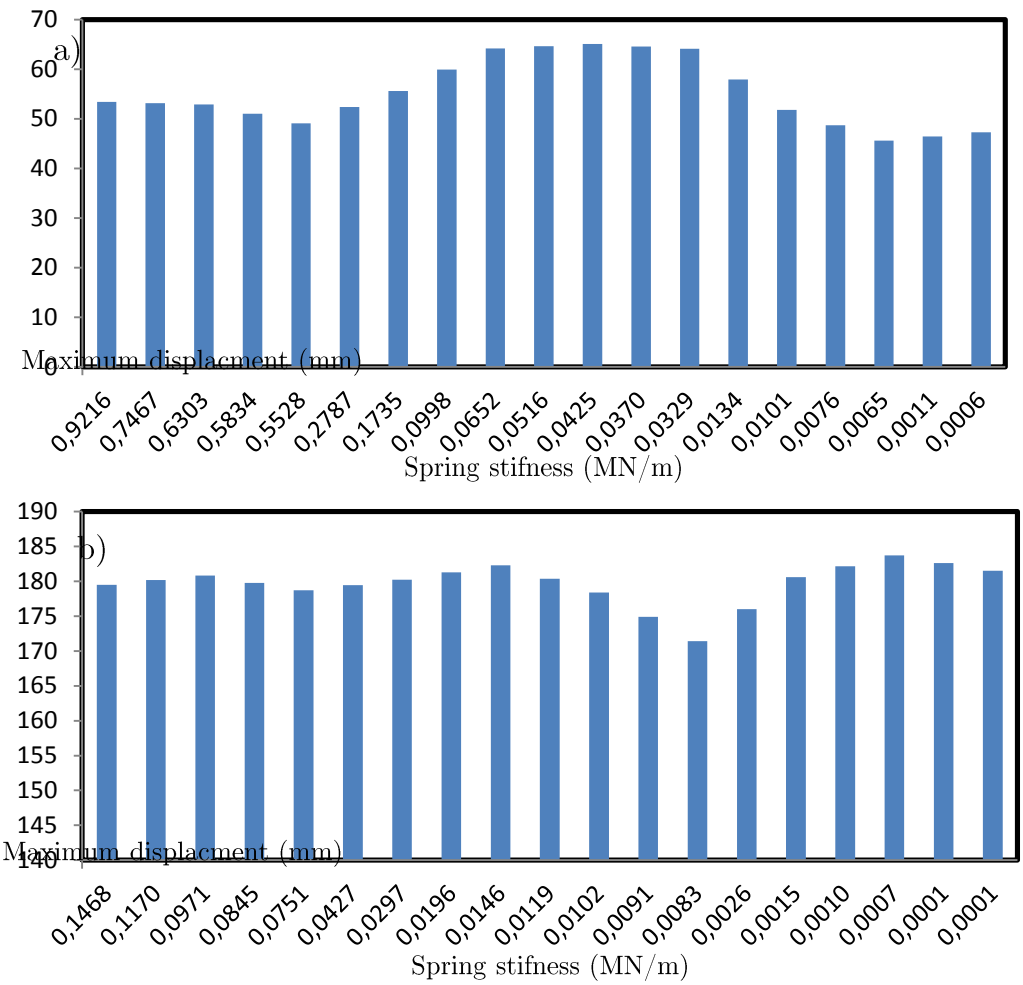

Figure 20: Maximum deformation vs. stiffness ratio, a) Impact velocity= 5 m/s b) Impact velocity=10 m/s

5 CONCLUSION

The effects of elastic support on impact characterization (the energy absorption, the peak load, etc.) of crash box were investigated in this study. The results showed that the stiffness of elastic support could change energy absorption and the maximum axial deformation. Further, it was confirmed that compared to a square crash box with the elastic support, a square crash box with the rigid wall support (the stiffness ratio≅0) absorbed more energy during the crash. The increasing spring stiffness leads to the increasing energy absorption. The results of the current study indicated that elastic and plastic elements (S-rail and firewall) in the bottom of crash box changed the behavior of crash box during the crash. This conclusion could be used in automotive design especially in designing those parts of vehicles responsible for causing destruction in the frontal crashes.

References

Abramowicz, W., Jones, N. (1986). Dynamic progressive buckling of circular and square tubes, International Journal of Impact Engineering 4(4): 243–70.

Abramowicz, W., Jones, N. (1984). Dynamic axial crushing of square tubes, International Journal Impact Engineering 2(2): 179–208.

Aktaya, L., Kröplin, B.H., Toksoy A.K., Güden, M. (2008). Finite element and coupled finite element/smooth particle hydrodynamics modeling of the quasi-static crushing of empty and foam-filled single, bitubular and constraint hexagonal- and square-packed aluminum tubes, International Journal Materials and Design 29(5): 952–962.

AlaviNia, A., FallahNejad, Kh., Badnava, H., Farhoudi, H.R. (2012). Effects of buckling initiators on mechanical behavior of thin-walled, International Journal of Thin-Walled Structures 59: 87–96.

Alexander, JM. (1960). An approximate analysis of the collapse of thin-cylindrical shells under axial loading The Quarterly Journal of Mechanics and Applied Mathematics 13 (1): 10-15

Almen, J.O., Laszlo, A. (1936). The uniform-section disk spring, ASME 58: 305–314.

Bouchet, J., Jacquelin, E., Hamelin, P. (2002). Dynamic axial crushing of combined composite aluminum tube, the role of both reinforcement and surface treatments, International Journal Composite Structures 56: 87–96.

El-Sobky, H., Singace, AA. (1999). Profiled polymer pipes as re-usable energy absorption elements, International Journal Mechanical Science 44: 1385–1400.

Galib, D Al., Limam, A., Combescure, A. (2006). Influence of damage on the prediction of axial crushing behavior of thin-walled aluminum extruded tubes, International Journal of Crashworthiness 11(1): 1-12.

Sun, G., Li, G., Hou, S., Zhou, S., Li, W., Li, Q. (2010). Crashworthiness design for functionally graded foam-filled thin-walled structures, A, International Journal Materials Science and Engineering 527(7-8): 1911–1919.

Güden, M., Kavi, H. (2006). Quasi-static axial compression behavior of constraint hexagonal and square-packed empty and aluminum foam-filled aluminum multi-tubes, International Journal Thin-Walled Structures 44(7): 739–750.

JandaghiShahi, V., Marzbanrad, J. (2012).Analytical and experimental studies on quasi-static axial crush behavior of thin-walled tailor-made aluminum tubes, International Journal of Thin-Walled Structures 60: 24–37.

Jing, Bi., Fang, H., Wang, Q., Ren, X. (2010). Modeling and optimization of foam-filled thin-walled columns for crashworthiness designs, Finite Elements in Analysis and Design 46(9): 698-709.

Jones, N. (1997). Structural Impact, Cambridge University Press.

Karagiozova, D., Alves, M. (2004). Transition from progressive buckling to global bending of circular shells under axial impact–Part I, Experimental and numerical observations, International Journal of Solids and Structures 41(5-6): 1565–1580.

Karagiozova, D., Jones, N. (2008). On the mechanics of the global bending collapse of circular tubes under dynamic axial load-Dynamic buckling transition, International Journal of Impact Engineering 35(5): 397–424.

Lankarani, HM., Ramalingam, VK. (2002). Analysis of impact on soft soil and its application to aircraft crashworthiness, International Journal of Crashworthiness, International Journal Crashworthiness 7(1): 57–65.

Lu, G., Yu, TX. (2003). Energy absorption of materials and structures, Woodhead Publishing, Cambridge; 268-373.

Mamalis, A.G., Manolakos, D.E., Ioannidis, M.B., Chronopoulos, D.G., Kostazos, P.K. (2009). On the crashworthiness of composite rectangular thin-walled tubes internally reinforced with aluminum or polymeric foams, Experimental and numerical simulation, Journal of Composite Structures 89(3): 416-423.

Marzbanrad, J., Abdollahpoor, A. and Mashadi, B. (2009). Effects of Triggering of Circular Aluminum Tubes on Crashworthiness, International Journal of Crashworthiness 14(6): 591-599.

Naghipour, P., Aktay, L., Johnson, A.F. (2008). Numerical investigation of structural crash response of thin-walled structures on soft soil, International Journal Materials and Design 29(10): 2052–2060.

Najafi,A.,Rais-Rohani, M. (2011). Mechanics of axial plastic collapse in multi-cell, multi-corner crush tubes, International Journal Thin-Walled Structures 49(1): 1–12.

Pugsley, SA. (1960). The crumpling of tubular structures under impact conditions. London, Proceeding of locomotive engineering. The Aluminum Development Association: 33–41.

Rossi, A., Behdinan, K. (2005). Numerical simulation of the axial collapse of thin-walled polygonal section tubes, International Journal Thin-Walled Structures 43(10): 1646–1661.

Salehghaffari, S., Tajdari, M., Panahi, M., Mokhtarnezhad, F., (2010). Attempts to improve energy absorption characteristics of circular metal tubes subjected to axial loading, International Journal of Thin-Walled Structures 48(6): 379–390.

Tadaharu Adachi, Atsuo Tomiyama, Wakako Araki, Akihiko Yamaji. (2008). Energy absorption of a thin-walled cylinder with ribs subjected to axial impact, International Journal of Impact Engineering 35(2): 65–79.

Zhang, X., Huh, H. (2009). Energy absorption of longitudinally grooved square tubes under axial compression, International Journal of Thin-Walled Structures 47(12): 1469–1477.

Zarei, H.R., Krogöer, M. (2006). Multi-objective crashworthiness optimization of circular aluminum tubes, International Journal of Thin-Walled Structures 44(3): 301–308.

Zhang A, Suzuki K. (2007). A study on the effect of stiffeners on quasi-static crushing of stiffened square tube with non-linear finite element method, International Journal Impact Engineering 34(3): 544–50.

Zhang, X.W., Tian, Q.D., Yu, T.X. (2009). Axial crushing of circular tubes with buckling initiators, International Journal of Thin-Walled Structures 47(6-7): 788–797.

Zhang, Y., Sun, G., Li, G., Luo, Z., Li, Q. (2012). Optimization of foam-filled bitubal structures for crashworthiness criteria, International Journal Materials and Design 38: 99-109.